Superconductivity in amorphous and microcrystalline transition-metal alloys*

W. L. Johnson and S. J. Poon

W. M. Keck Laboratory of Engineering Materials, California Institute of Technology, Pasadena, California 91109
(Received 2 October 1974)

Results of x-ray diffraction, electrical resistivity, critical magnetic field, and transport measurements for several bulk amorphous and microcrystalline transition-metal superconductors obtained by liquid quenching are presented and discussed. Simple J_c-H_{c2}-T_c relations are observed for this class of materials. A linear relation between electronic diffusivity and nearest-neighbors distance is derived from critical field measurements. The relationship between the formation of an amorphous phase by rapid cooling from the liquid state, lattice stability, and the characteristics of phase diagrams are discussed.

PACS numbers: 74.50.R, 74.10., 81.50.S

I. INTRODUCTION

Superconductivity in amorphous metal films obtained by vapor quenching has been reported in the literature.[1-3] In a recent paper, superconductivity in bulk amorphous Au-La alloys obtained by liquid quenching was reported by the authors.[4] It was suggested that an investigation be made to determine whether bulk amorphous superconducting binary alloys containing only transition metals could be prepared using the liquid quenching technique.

In the present paper, experimental results for amorphous and microcrystalline alloys of Au-La, Nb-Ni, Nb-Rh, and Pd-Zr are presented. The distinction between amorphous and microcrystalline alloys is discussed. It is shown that these phases can each be characterized by a well-defined superconducting transition temperature T_c. The observed dependence of the upper critical field $H_{c2}(T)$ and the transport behavior $[J_c(H), J_c(T)]$ are found to be general properties of this class of materials.

It has been suggested that the problem of high-temperature superconductivity is related to crystal lattice instability. McMillan[5] has shown how softening of phonon modes and the accompanying lattice instability can lead to an increase in T_c. The formation of a nonequilibrium amorphous or microcrystalline phase in a binary alloy as a result of liquid quenching is related to the intrinsic lattice instability of the associated equilibrium crystalline phases. This relationship is discussed in terms of phase diagrams. Several factors which are important in determining the superconducting transition temperature of an amorphous phase are pointed out. It is found that the transition temperature of an amorphous phase obtained by liquid quenching is always less than that of one of the related crystalline phases.

II. EXPERIMENTAL PROCEDURES

A study was made on the binary alloy systems Au-La, Nb-Ni, Nb-Rh, and Pd-Zr. For the Au-La system, a detailed description has been given in Ref. 4. The Nb-Ni and Pd-Zr systems were investigated for compositions within the ranges of formation of microcrystalline phases as described by Giessen.[6] The $Nb_{100-x}Rh_x$ alloys were studied with $38 \leq x \leq 50$. In addition an alloy $Nb_{56}Ni_{16}Rh_{28}$ was prepared. Alloys were prepared by induction melting of the appropriate constituents on a silver boat under an argon atmosphere. Samples used for experimental measurements were obtained by quenching small amounts (~ 10 mg) of the alloys from the liquid state following a technique described in Ref. 7. The samples obtained by this technique are in the form of foils having an area in the order of 1 cm^2 and a nonuniform thickness of less than 10 μm. The structure of every foil was checked by taking diffraction patterns with a Norelco diffractometer (Cu$K\alpha$ radiation). The samples were scanned through a range of 2θ angles from 25° to 60°. An x-ray diffraction study of annealed samples was also used to determine the characteristic temperatures at which transformation to more stable crystalline phases takes place. Electrical resistance as a function of temperature was measured using a standard four-probe technique. The temperature was determined by using a germanium resistance thermometer with an accuracy of 0.02 °K. Critical magnetic field measurements were performed using a superconducting solenoid for magnetic fields up to 40 kG oriented transversely to the sample and temperatures down to 1.85 °K. The temperature for H_{c2} measurements was determined by measuring the vapor pressure over the liquid He^4 bath. Critical current density J_c measurements for $Au_{24}La_{76}$ and $Nb_{58}Rh_{42}$ alloys were made as a function of temperature and magnetic field using the same experimental apparatus for the H_{c2} measurements. All transport measurements presented are for fields oriented transversely to the direction of current flow.

III. EXPERIMENTAL RESULTS

A. Structure analysis

A summary of x-ray diffraction results for the amorphous and microcrystalline phases is given in Table I.

TABLE I. Summary of x-ray diffraction results.

Alloy	Nearest-neighbor distance (Å)	Effective microcrystal size (Å)
$Au_{24}La_{76}$	3.55	17.5
$Nb_{58}Rh_{42}$	2.73	24
$Nb_{56}Ni_{16}Rh_{28}$	2.66	18
$Nb_{60}Ni_{40}$	2.66	20
$Pd_{30}Zr_{70}$	3.00	27

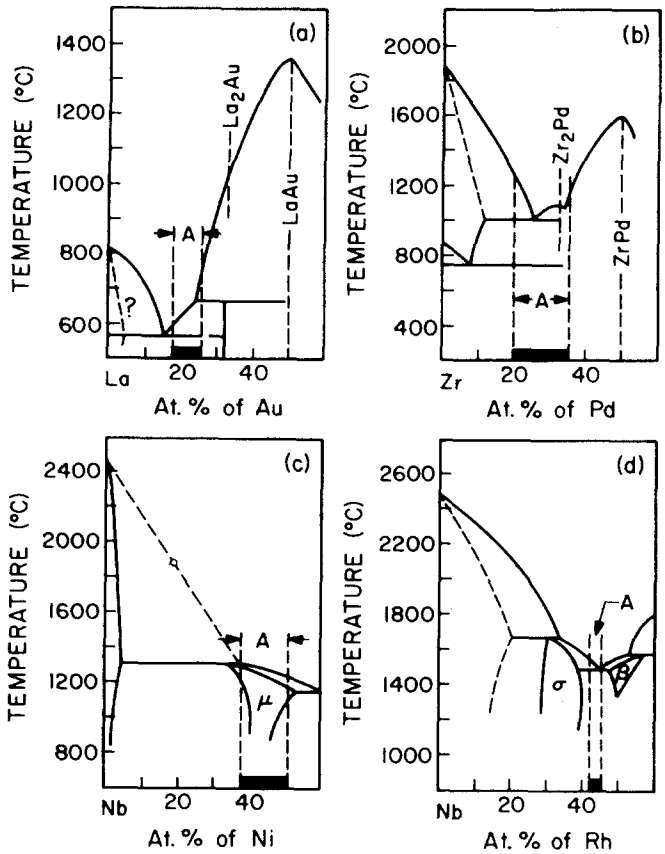

FIG. 1. Phase diagrams for Au-La, Nb-Ni, Nb-Rh, and Pd-Zr systems. Shaded regions indicate compostion ranges where single amorphous and microcrystalline phases can be obtained by liquid quenching.

In Fig. 1, the composition ranges for amorphous and microcrystalline phases is shown. The composition ranges for the formation of micrystalline phases in the Nb-Ni and Pd-Zr systems are found to be nearly identical to those given by Giessen. A single microcrystalline phase was observed in $Nb_{100-x}Rh_x$ for $42 \leq x \leq 45$. The nearest-neighbor distance (NND) and the effective microcrystal size (μ_{eff}) given in Table I were calculated from the Debye formula[8] and the Sherrer formula, respectively. The effective microcrystal sizes ranges from 4.9NND to 9NND. Previously reported amorphous metal alloys obtained by liquid quenching can all be characterized by μ_{eff} ranging from 4NND to 5.5NND.[9] When μ_{eff} exceeds ~6NND, it is no longer clear that the term amorphous can be used to describe the structure of the phase. Using this rather arbitrary criterion implies that of the alloys studied, only Au-La alloys can be described as amorphous while the rest of the alloys should appropriately be described as microcrystalline. For a detail description of the related crystal structures in the Au-La, Nb-Ni, Pd-Zr, and Nb-Rh alloy systems, the reader should refer to Refs. 4, 6, 10, and 11. Samples of each alloy studied were annealed at temperatures varying from 100 to 850 °C to determine the characteristic crystallization temperature. The microcrystalline samples of $Pd_{30}Zr_{70}$ and $Nb_{60}Ni_{40}$ were found to decompose into more stable crystalline phases after annealing for periods of the order of 24 h at temperatures of ~300 and 600 °C, respectively, in agreement with Ref. 6. The characteristic annealing temperature for $Nb_{58}Rh_{42}$ was found to be ~650 °C. Annealing at this temperature for one day results in the decomposition of the micrystalline phase into the crystalline phases described in the equilibrium phase diagrams.

B. Electrical resistivity measurements

The resistivity $\rho(T)$ for amorphous $Au_{24}La_{76}$ and microcrystalline $Nb_{58}Rh_{42}$ together with that of crystalline samples are presented in Figs. 2(a) and 3(a), respectively. The crystalline samples were prepared by liquid quenching the alloys at a cooling rate insufficient to yield an amorphous or a microcrystalline phase. All of the alloys in Table I can be characterized by a well-defined T_c with a transition width ΔT_c less than 0.4 °K. The T_c for $Nb_{60}Ni_{40}$ and $Pd_{30}Zr_{70}$ were found to be 1.5 and 2.4 °K, respectively. Detailed results of electrical resistivity measurements for amorphous Au-La alloys can be found in Ref. 4. The temperature coefficient of resistivity $(1/\rho_0)[d\rho(T)/dT]$ (where ρ_0 is the residual resistivity at 10 °K) for Au_xLa_{100-x} measured from room temperature to low temperatures is found to vary from $\sim -10^{-4}/°K$ for $x = 16$ to $\sim +10^{-4}/°K$ for $x = 24$. The observed change in sign of the temperature coefficient of resistivity as a function of composition has been discussed in the literature for amorphous alloys.[12] It is difficult to determine accurately the resistivity of samples prepared using the "gun" technique due to the nonuniform thickness of the samples. Values of ρ_0 were obtained by estimating the average sample thickness based on sample weight per unit area with the assumption that

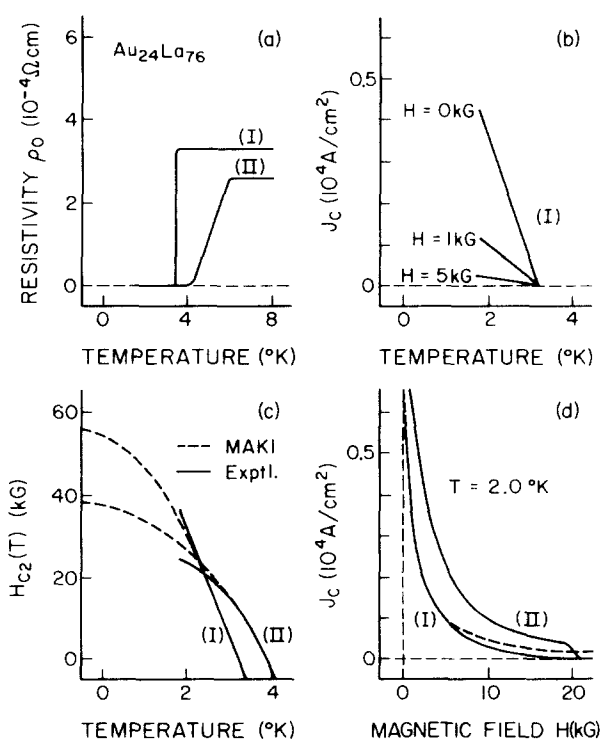

FIG. 2. Results of electrical resistivity, critical magnetic field, and transport properties measurements for (I) amorphous and (II) highly crystallized $Au_{24}La_{76}$ alloys.

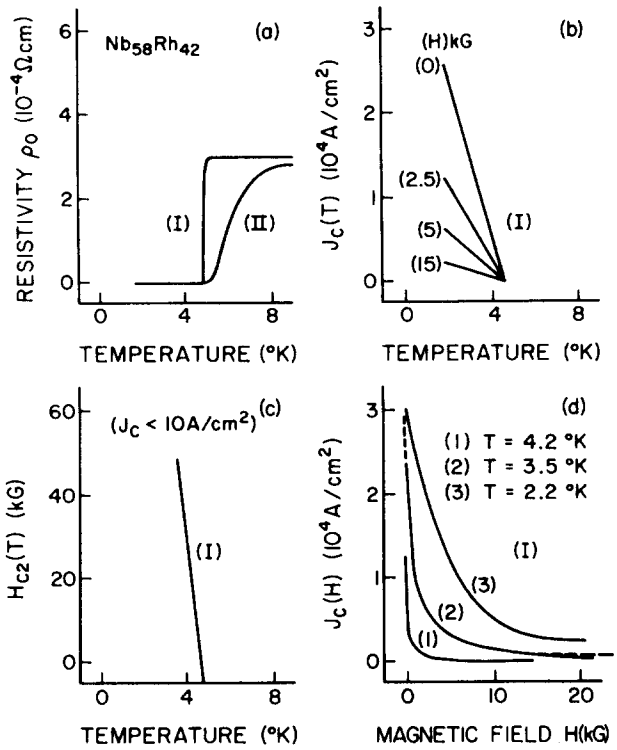

FIG. 3. Results of electrical resistivity, critical magnetic field, and transport properties measurements for (I) microcrystalline $Nb_{58}Rh_{42}$ alloy. Result of electrical resistivity measurement for (II) highly crystallized $Nb_{58}Rh_{42}$ alloy is also included in (a).

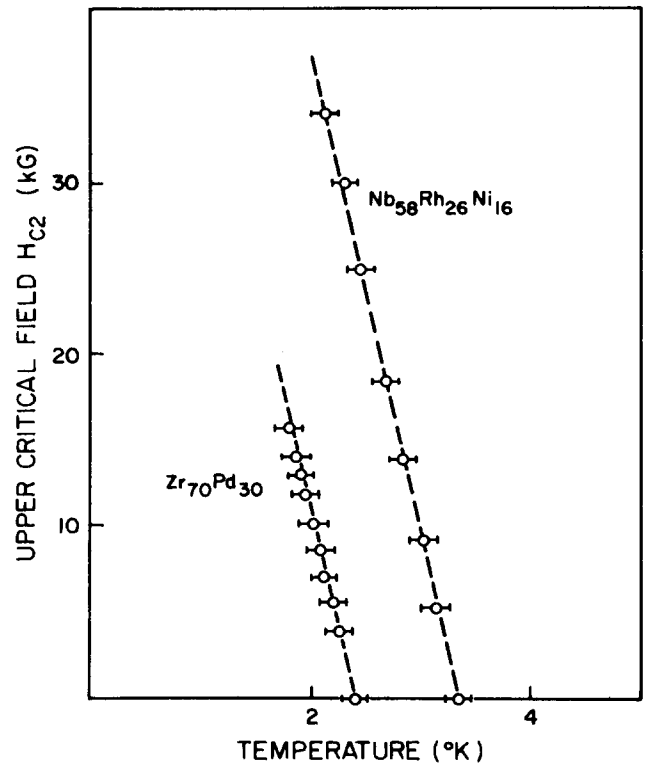

FIG. 4. Critical field H_{c2} as a function of temperature for $Nb_{56}Ni_{16}Rh_{28}$ ($T_c \simeq 3.4$°K) and $Pd_{30}Zr_{70}$ ($T_c \simeq 2.4$°K) microcrystalline alloys.

the material density is nearly that of the associated crystalline phase. The residual resistivity and temperature coefficient of resistivity calculated in this way for the microcrystalline phases are all found to be of the order of 3×10^{-4} Ωcm and 10^{-4}/°K, respectively. These values are typical of those observed in amorphous alloys.

C. Critical magnetic field and transport properties

The upper critical field $H_{c2}(T)$ was measured for all alloys except $Nb_{60}Ni_{40}$ ($T_c \sim 1.5$ °K), the low T_c of which made measurement of H_{c2} impractical. The $H_{c2}(T)$ curves for amorphous $Au_{24}La_{76}$ and microcrystalline $Nb_{58}Rh_{42}$ are shown in Figs. 2(c) and 3(c), respectively. The $H_{c2}(T)$ curves for other alloys are shown in Fig. 4. Linear behavior was observed in the amorphous and microcrystalline samples throughout the measured ranges of temperature and magnetic field. This behavior is apparently general for this class of materials. In Fig. 2(c), reproduced from Ref. 4, the dashed lines were obtained by fitting the data to the Maki theory.[13] The gradient $[-dH_{c2}(T)/dT]_{T=T_c}$ evaluated for the alloys studied is plotted as a function of nearest-neighbor distance (NND) in Fig. 5, and an inverse relation is observed. This relation will be discussed later.

Critical current density $J_c(T)$ measurements as a function of temperature in a constant magnetic field for amorphous $Au_{24}La_{76}$ and microcrystalline $Nb_{58}Rh_{42}$ are shown in Figs. 2(b) and 3(b). The behavior of $J_c(T)$ was found to be linear for both alloys over the temperature range investigated. Critical current density measurements as a function of magnetic field at constant temperature $J_c(H)$ are shown in Figs. 2(d) and 3(d) for these samples and also for the partially crystallized sample of $Au_{24}La_{76}$ quenched at a cooling rate insufficient to

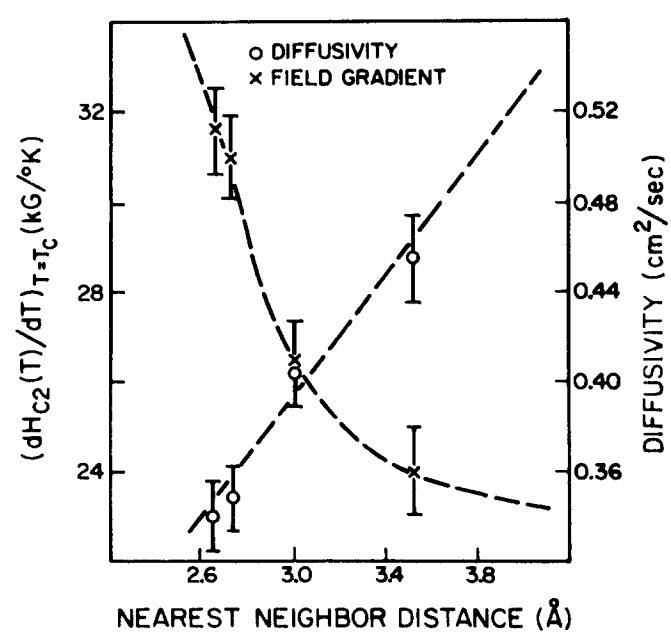

FIG. 5. Critical field gradient for amorphous $Au_{24}La_{76}$, microcrystalline $Nb_{56}Ni_{16}Rh_{28}$, $Nb_{58}Rh_{42}$, and $Pd_{30}Zr_{70}$ alloys as a function of nearest-neighbor distance. Electronic diffusivity for the same alloys as a function of NND is also presented.

TABLE II. Approximate vlaues of $\alpha_c/(1-t)^2$ obtained from hyperbolic fit of J_c-H_{c2} data for $Nb_{58}Rh_{42}$ microcrystalline alloy ($T_c \simeq 4.7$ °K).

T (°K)	$\alpha_c(T)$ (10^6 A G/cm^2)	$\alpha_c(T)/(1-t)^2$ (10^8 A G/cm^2)
2.2	60	2.1
3.5	16	2.4
4.2	2	1.8

yield an amorphous phase. The transitions from the superconducting to the normal state were reversible for the amorphous $Au_{24}La_{76}$ and microcrystalline $Nb_{58}Rh_{42}$. For the crystallized $Au_{24}La_{76}$, the transition is not reversible and the behavior of $J_c(H)$ indicates that flux pinning takes place in this sample. For the amorphous $Au_{24}La_{76}$ and microcrystalline $Nb_{58}Rh_{42}$ samples, $J_c(H)$ varies approximately like H^{-1}, which is characteristic of an ideal type-II superconductor. The maximum measured values of J_c (at $T \sim 2$ °K and zero field) are about 10^4 A/cm^2 for amorphous $Au_{24}La_{76}$ and 3×10^4 A/cm^2 for microcrystalline $Nb_{58}Rh_{42}$.

IV. DISCUSSION

A. Electromagnetic properties

The magnetic properties and the characteristic intrinsic parameters coherence length ξ, penetration depth λ, and the electronic mean free path l_{mfp} of the amorphous Au-La alloys were discussed in Ref. 4. It was pointed out that the type-II behavior can be characterized by a very large Ginzburg-Landau parameter $\kappa \sim 70$. A similar argument base on the measured residual resistivity ρ_0 and the measured values of H_{c2} can be used to show that comparable values of κ must be used to characterize the other alloys of this study. Details will not be given here. The linearity of $H_{c2}(T)$ observed for all amorphous and microcrystalline alloys can be explained using the Maki Theory[13] and Werthamer's extension[14] of Maki's work to include the paramagnetic effect and the spin-orbit scattering effect. It was pointed out in Ref. 4 that the spin-orbit scattering effect is probably responsible for the observed linearity of H_{c2} over a wide temperature range in amorphous and microcrystalline alloys.

In Fig. 5, an inverse relation between $[-dH_{c2}(T)/dT]_{T=T_c}$ and NND can be seen. It is worthwhile to examine this relation in further detail. Using Maki's expression[12]

$$\log(1/t) = \Psi(1 + eDH_{c2}/2\pi c k_B T_c t) - \Psi\tfrac{1}{2} \qquad (1)$$

which relates H_{c2} and $t = T/T_c$, one can calculate the electronic diffusivity $D = \frac{1}{3}v_F l_{mfp}$ required to fit the observed $H_{c2}(T)$ curves. This is most easily accomplished by taking the limiting case $t \to 1$ for which Eq. (1) reduces to

$$H_{c2}(t) = \frac{4k_B T_c}{\pi e}\left(\frac{c}{D}\right)(1-t)\left[1-\left(\frac{1}{2}-\frac{28}{\pi^4}\xi(3)\right)(1-t)\right]. \qquad (2)$$

It then follows that

$$\left(\frac{dH_{c2}(T)}{dT}\right)_{T=T_c} = -\frac{4k_B c}{\pi e D}. \qquad (3)$$

This expression should be valid for the present case where $l_{mfp} \ll \xi_0$ as discussed in Ref. 4. Using the observed values of $[-dH_{c2}(T)/dT]_{T=T_c}$, one can calculate the electronic diffusivity D for the amorphous and microcrystalline alloys. These results are shown in Fig. 5. A linear relation between D and NND is observed. A straight line of the form $D = 0.134\text{NND} - 0.014$ is obtained by using the least-squares fit. Although the plot is based on limited data, it suggests that this may be a general characteristic of bulk amorphous and microcrystalline transition-metal superconductors. It is interesting to note that the straight line obtained from the least-squares fit gives $D \approx 0$ as NND $\to 0$. Since for an extremely disordered material, $p_F l_{mfp} = m^* v_F l_{mfp} \sim \hbar$ (where m^* is the effective mass of the electron), one expects $D = \frac{1}{3}v_F l_{mfp} \sim \hbar/3m^*$. The relationship between D and NND could then be interpreted as a linear dependence of $1/m^*$ on NND. The degree of localization of d-electron bonding states is related to m^* and to the bond lengths (NND). It is significant that the melting temperature of the alloys increases (indicating increased bonding strength) as NND decreases. Further investigation of this problem is clearly necessary and may give useful insight into the fundamental electronic properties of this class of materials.

The observed behavior of $J_c(H)$ at fixed temperatures for $Au_{24}La_{76}$ and $Nb_{58}Rh_{42}$ are now discussed. For the amorphous and microcrystalline alloys, the lattice is disordered on a scale much smaller than the coherence length ξ so that favorable centers for flux pinning do not exist. In the absence of flux pinning, the behavior of $J_c(H)$ is determined by the Lorentz force so that an inverse relation between J_c and H is expected for $H > H_{c1}$.[15] For the present case, H_{c1} is expected to be very small ($H_{c1} \sim 10$ G since $\kappa \sim 70$) and thus a H^{-1} dependence of J_c is expected for $H \gtrsim 10$ G. The data can be fitted using the expression $J_c(T)H_{c2}(T) = \alpha_c(T)$, where $\alpha_c(T)$ is a temperature-dependent constant to be determined. Typical values of α_c for amorphous $Au_{24}La_{76}$ and microcrystalline $Nb_{58}Rh_{42}$ obtained by fitting the data in this manner are $\alpha_c(T = 2\ °K) \simeq 5\times10^6$ A G/cm^2 and $\alpha_c(T = 3.5\ °K) \simeq 1.6\times10^7$ A G/cm^2, respectively. The fitted curves are shown in Figs. 2(d) and 3(d), and good agreement with experiments is obtained over a broad range of magnetic fields ($H \lesssim 10$ kG). By comparison, the partially crystallized sample of $Au_{24}La_{76}$ exhibits noticeable flux pinning behavior.

The observed linear behavior of $J_c(T)$ for constant H along with the relation $J_c(T)H_{c2}(T) = \alpha_c(T)$ implies that α_c has the temperature dependence $\alpha_c(t) \sim (1-t)^2$ over the observed temperature range. This relation can be simply checked by comparing the value of $\alpha_c(t)$ at various temperatures. For $Nb_{58}Rh_{42}$, this comparison is illustrated in Table II by evaluating the ratio $\alpha_c(t)/(1-t)^2$ which is seen to be roughly constant.

B. Lattice instability and superconductivity

The phase diagrams of the four alloy systems studied are shown in Fig. 1 along with the range over which an amorphous or microcrystalline phase is obtained by quenching. It is clear that the formation of these phases is related to features of the equilibrium phase diagrams.

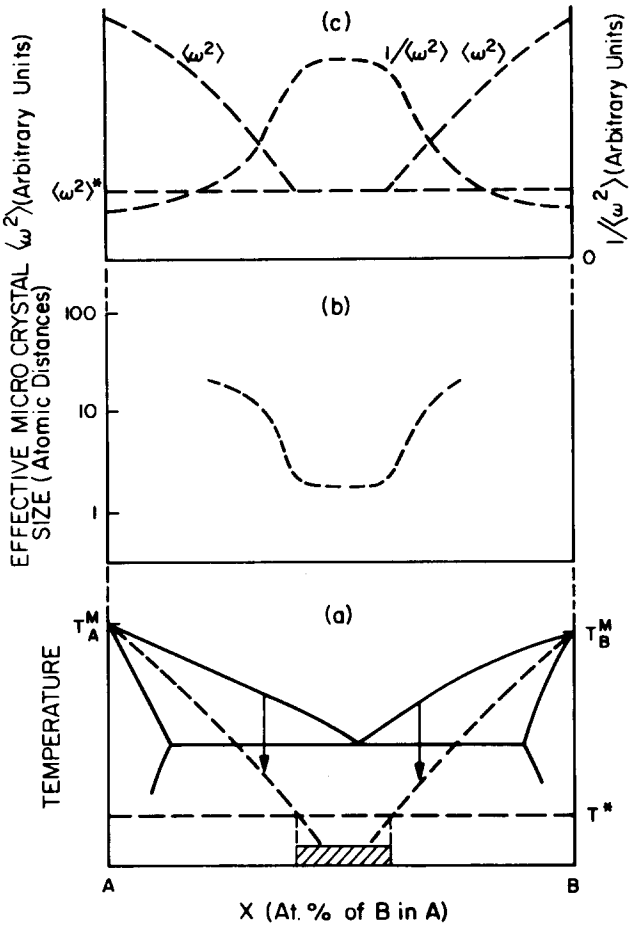

FIG. 6. General features characterizing the formation of an amorphous phase. Solid lines in (a) indicate the equilibrium liquidus, solidus, and terminal solubility curves. Dashed lines indicate effects due to rapid cooling from the liquid state.

First, these phases are obtained for compositions at which the liquidus temperature in the phase diagram has a pronounced minimum as a function of composition. One or more discontinuities in the slope of the liquidus are observed in the composition range. Second, on either side of the amorphous phase range, stable equilibrium crystal structures which form congruently from the melt can be found. The minimum and the discontinuities in the liquidus can be related to the changeover in the equilibrium crystal structure as a function of composition. For example, in the Au-La system, the related crystal structures are β-La with a melting temperature $T^M = 812\,^\circ$C and the equiatomic compound AuLa with $T^M = 1360\,^\circ$C. The liquids falls to a eutectic minimum $T_e = 560\,^\circ$C at the composition $Au_{16}La_{84}$ and discontinuities in the slope are observed at 16 and 25 at.% Au in La. The amorphous phase is observed from 18 to 26 at.% Au.

The general features characterizing the formation of the amorphous phases are illustrated schematically in Fig. 6. In Fig. 6(a), a typical portion of a phase diagram illustrating the liquidus, solidus, and terminal solubility curves is shown. Stable crystalline phases A and B are characterized by melting temperatures T_A^M and T_B^M. The dashed lines illustrate the liquidus obtained by supercooling. The supercooled liquid solidifies at a characteristic temperature T^* forming an amorphous or microcrystalline phase. On either side of the amorphous phase range, the degree of supercooling is not sufficient to suppress microcrystalline growth of the phases A and B. Figure 6(b) illustrates the qualitative behavior of the effective microcrystal size as a function of composition for the liquid quenched alloys. The decreased melting temperature and decreased stability of the crystalline phases obtained over an extended homogeneity range can be characterized by a decreased mean square phonon frequency $\langle\omega^2\rangle$. In Fig. 6(c), the qualitative behavior of $\langle\omega^2\rangle$ and $1/\langle\omega^2\rangle$ as a function of composition expected for the liquid quenched alloys is illustrated. Experimental evidence for reduced $\langle\omega^2\rangle$ in liquid quenched amorphous alloys has been reported.[16] McMillan has discussed the relationship between $\langle\omega^2\rangle$ and the electron-phonon coupling strength λ and has argued that for a given crystal structure $\lambda \sim 1/\langle\omega^2\rangle$. The behavior of λ is not clear in the present case since the electronic structure of the amorphous phase may be very different from that of the associated crystalline phases. It is clear that electron-lattice scattering will be greatly enhanced due to the high degree of disorder. The residual resistivity $\rho_0 \sim 3\times10^{-4}\ \Omega$cm observed for these alloys provides strong evidence for this. The density of states at the Fermi level will be limited by the absence of long-range order as discussed by Strongin in his thin-film work.[17] The small microcrystal size μ_{eff} will limit the phonon mean free path l_{ph} to ~20 Å (6NND). Finally, the effect of thermodynamic fluctuation in microcrystallites should not be neglected as pointed out in Ref. 17. These factors can all play a role in determining the superconducting transition temperature of the amorphous phase. Concerning the observed superconducting transition temperatures of the amorphous phases, the following can be said. The highest T_c observed in the amorphous and microcrystalline phases of the present study is of the order of or less than half of the miximum T_c obtained in a related crystalline phase. For amorphous $Au_{24}La_{76}$, $T_c \simeq 3.3\,^\circ$K, while $T_c \simeq 6\,^\circ$K for β-La. For $Nb_{58}Rh_{42}$, a transition temperature of $10.3\,^\circ$K is obtained after annealing the amorphous samples.[18] The annealed samples have a σ-phase related structure. For microcrystalline $Nb_{58}Rh_{42}$, $T_c \simeq 4.7\,^\circ$K. The equilibrium alloy $Pd_{10}Zr_{90}$ has $T_c \simeq 7.5\,^\circ$K, while the microcrystalline alloy has $T_c \simeq 2.4\,^\circ$K. Collver and Hammond[3] have reported the behavior of T_c for highly disordered $4d$ and $5d$ transition-metal alloy films obtained by vapor quenching. They found that T_c is a triangular function of the average number of electrons per atom (e/a) peaking at $T_c \simeq 10\,^\circ$K near midseries. The transition temperature of the present alloys is generally lower than those predicted by the curves in Ref. 3 at the corresponding e/a values. This difference may be related to the fact that Ref. 3 considered alloys of neighboring elements in the periodic table, while the present results concern binary alloys with constitutents further separated.

ACKNOWLEDGMENT

The authors wish to express their appreciation to Professor Pol Duwez for his support and encouragement throughout this work.

*Work supported by the U.S. Atomic Energy Commission.

[1]W. Buckel and R. Hilsch, Z. Phys. **138**, 109 (1954).
[2]W. Buckel and R. Hilsch, Z. Phys. **138**, 118 (1954).
[3]M.M. Collver and R.H. Hammond, Phys. Rev. Lett. **30**, 92 (1973).
[4]W.L. Johnson, S.J. Poon, and P. Duwez, Phys. Rev. B **11**, 150 (1975).
[5]W.L. McMillan, Phys. Rev. **167**, 331 (1968).
[6]R. Ray, B.C. Giessen, and N.J. Grant, Scr. Metall. **2**, 357 (1968).
[7]P. Duwez, *Progress in Solid State Chemistry* (Pergamon, Oxford, 1966), Vol. 3.
[8]The calculation of NND (or closest distance of approach) for liquids and amorphous solids is given by A. Guinier, *X-Ray Diffraction* (W.H. Freeman and Co., San Francisco, 1963).
[9]R.C. Crewdson, Ph.D. thesis (California Institute of Technology, 1968) (unpublished).
[10]R.C. Ruhl, B.C. Giessen, M. Coher, and N.J. Grant, Acta Mettall. **15**, 1693 (1967).
[11]F.A. Shunk, *Constitution of Binary Alloys, Second Supplement* (McGraw-Hill, New York, 1969).
[12]A.K. Sinha, Phys. Rev. **1**, 4541 (1970).
[13]K. Maki, Physics **1**, 127 (1964).
[14]E. Helfand and N.R. Werthamer, Phys. Rev. **147**, 288 (1966).
[15]D. Saint-James, G. Sarma, and E.J. Thomas, *Theory of Type II Superconductivity* (Pergamon, Oxford, 1969).
[16]Brage Golding, B.G. Bagley, and F.S.L. Hsu, Phys. Rev. Lett. **29**, 68 (1972).
[17]M. Strongin, Physica **55**, 155 (1971).
[18]W.L. Johnson and S.J. Poon, J. Appl. Phys. (to be published).